Compartmentalization of the endoplasmic reticulum in the early *C. elegans* embryos

Zuo Yen Lee,[1] Manoël Prouteau,[2] Monica Gotta,[2] and Yves Barral[1]

[1]Department of Biology, Institute of Biochemistry, Swiss Federal Institute of Technology Zürich, CH-8093 Zürich, Switzerland
[2]Department of Cell Physiology and Metabolism, University of Geneva Medical School, CH-1211 Geneva, Switzerland

The one-cell *Caenorhabditis elegans* embryo is polarized to partition fate determinants between the cell lineages generated during its first division. Using fluorescence loss in photobleaching, we find that the endoplasmic reticulum (ER) of the *C. elegans* embryo is physically continuous throughout the cell, but its membrane is compartmentalized shortly before nuclear envelope breakdown into an anterior and a posterior domain, indicating that a diffusion barrier forms in the ER membrane between these two domains. Using mutants with disorganized ER, we show that ER compartmentalization is independent of the morphological transition that the ER undergoes in mitosis. In contrast, compartmentalization takes place at the position of the future cleavage plane in a *par-3*–dependent manner. Together, our data indicate that the ER membrane is compartmentalized in cells as diverse as budding yeast, mouse neural stem cells, and the early *C. elegans* embryo.

Introduction

The ER is an extensive network of membranous tubules and sheet-like cisternae that extends throughout the cytoplasm. In most cell types, the ER is a single membranous entity delimiting a single luminal space in the cell (Terasaki and Jaffe, 1991; Feng et al., 1994; Jaffe and Terasaki, 1994; Terasaki, 2000; Luedeke et al., 2005; Puhka et al., 2007). Yet, the ER is divided into morphologically and functionally diverse domains, such as the RER involved in co-translational translocation of proteins of the trafficking pathway into the ER (Blobel and Dobberstein, 1975a,b; Walter and Blobel, 1981; Walter et al., 1981), the smooth ER essential for the synthesis of numerous lipids (Dennis and Kennedy, 1972; Vidugiriene et al., 1999; Baumann and Walz, 2001), and the nuclear envelope. The distinction between these domains relies on the contribution of many proteins organizing the ER into domains of unique shapes and functions (Baumann and Walz, 2001; Voeltz et al., 2002; English and Voeltz, 2013). The contact sites between the extensive ER network and other membrane systems (Levine and Rabouille, 2005; English and Voeltz, 2013) contribute to the further organization of the ER into functionally distinct microdomains. In budding yeast and dividing neural stem cells, diffusion barriers also impose a higher order organization on the ER by compartmentalizing it into large domains roughly corresponding to future daughter cells (Luedeke et al., 2005; Clay et al., 2014; Moore et al., 2015).

The one-cell *Caenorhabditis elegans* embryo is polarized. Upon fertilization, cortical contraction directed toward the anterior pole and powered by the actomyosin cytoskeleton localizes PAR-3, PAR-6, and PKC-3 (Etemad-Moghadam et al., 1995; Watts et al., 1996; Tabuse et al., 1998) proteins to the anterior cortical pole of the embryo, whereas PAR-1 and PAR-2 (Guo and Kemphues, 1995; Boyd et al., 1996) proteins occupy the posterior cortex (Munro et al., 2004; Motegi and Sugimoto, 2006; Motegi and Seydoux, 2013). Reciprocal exclusion between the PAR-3/PAR-6/PKC-3 complex and PAR-2/PAR-1 ensures the separation and maintenance of the anterior and posterior cortical domains. PAR proteins promote the partition of the polarity mediator MEX-5/6 to the anterior and of the cell fate determinant PIE-1 to the posterior cytoplasm. Polarity is maintained until the end of the first division, where the embryo divides unequally, giving rise to a larger anterior blastomere, called AB, and a smaller posterior blastomere, called P1 (Rose and Gönczy, 2014).

The reorganization of the ER in *C. elegans* embryos during the first cell cycle is also PAR and actin dependent (Poteryaev et al., 2005). In wild-type one-cell embryos, the ER is enriched in the anterior domain. This asymmetry is abolished in *par-3* and *par-6* knockdown as well as in latrunculin A–treated embryos (Poteryaev et al., 2005). In this study, we used physical methods to characterize ER organization in the embryo and to ask if compartmentalization of the ER membrane is conserved in *C. elegans*.

Correspondence to Yves Barral: yves.barral@bc.biol.ethz.ch

M. Prouteau's present address is Dept. of Molecular Biology, Sciences III, University of Geneva, CH-1211 Geneva, Switzerland.

Abbreviations used: AI, anisotropy index; A-P, anteroposterior; FLIP, fluorescence loss in photobleaching; NEBD, nuclear envelope breakdown; PNM, pronuclear meeting; ROI, region of interest.

The Rockefeller University Press $30.00
J. Cell Biol. Vol. 214 No. 6 665–676
www.jcb.org/cgi/doi/10.1083/jcb.201601047

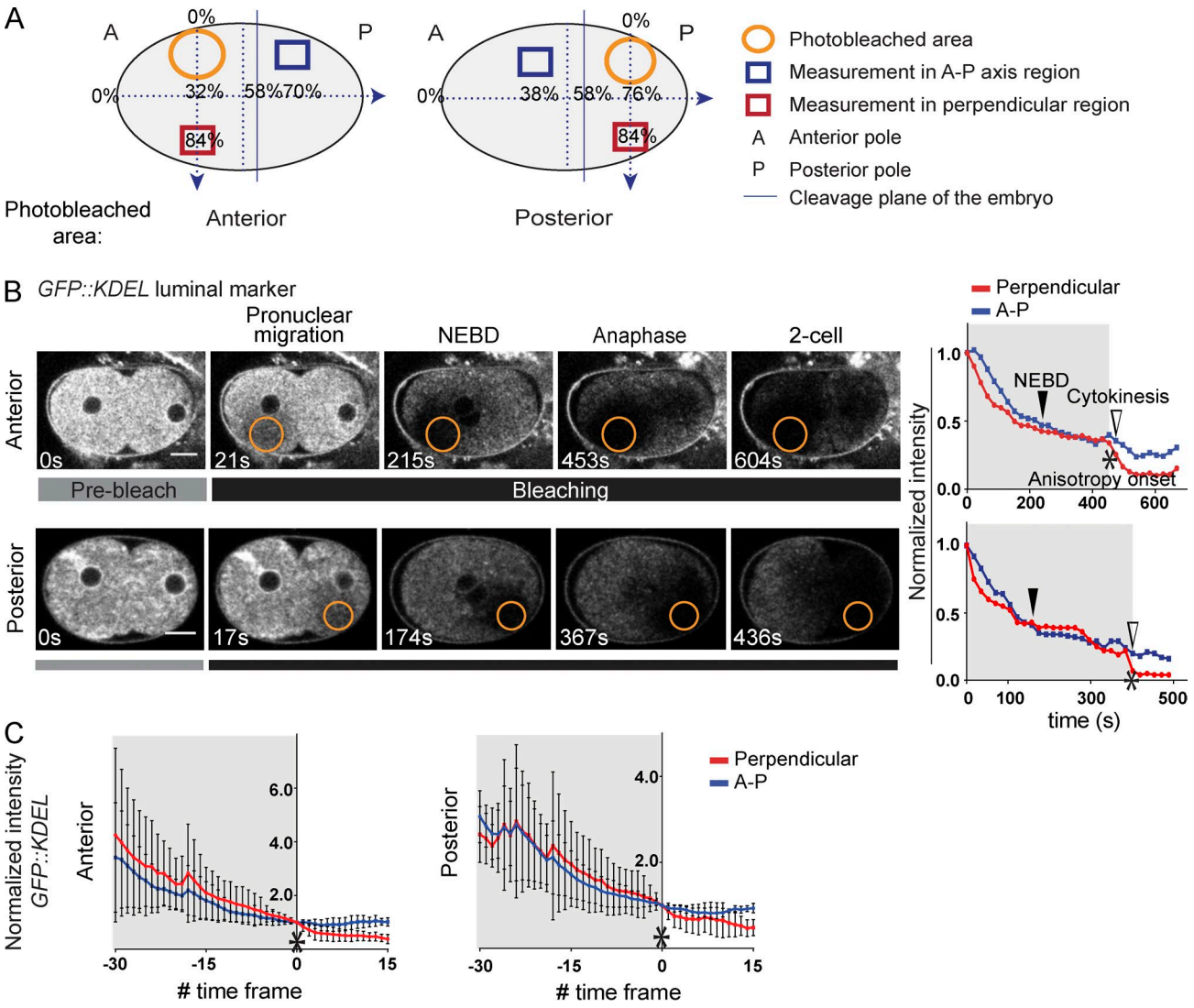

Figure 1. **The ER in the *C. elegans* embryo is continuous.** (A) Schematics illustrate the photobleached area (orange circles), the measurement regions in the A-P (blue squares) and perpendicular (red squares) directions, and their positions in percent egg length. The solid vertical lines represent the positions of the cleavage plane, determined by referring to the last frame of the video when the embryo has divided. The dotted vertical lines indicate the middle positions of the A-P axis of the embryo. (B) Confocal images of the FLIP experiments (left) and quantification (right) of a representative embryo for the *GFP::KDEL* photobleached in the anterior or the posterior domain. Gray bars indicate the prebleached first images; black bars indicate repeated bleaching in the remainder of the indicated cell cycle. The graphs for each embryo shown represent the kinetics of fluorescence loss for the corresponding embryo. The black arrowheads indicate NEBD; the white arrowheads indicate cytokinesis; gray shaded areas show the period of isotropic diffusion; asterisks show the anisotropy onset. Also see Videos 1 and 2. Bars, 10 µm. (C) Graphs of the kinetics of fluorescence loss of *GFP::KDEL* embryos with the alignment to the time point of anisotropy onset. Asterisks show the anisotropy onset. $n_{anterior}$ = 15; $n_{posterior}$ = 14. Mean ± SD.

Results and discussion

The ER in the embryo is continuous

The ER is continuous throughout the cell in many eukaryotes (Feng et al., 1994; Terasaki, 2000; Luedeke et al., 2005; Puhka et al., 2007; Moore et al., 2015). To test whether the ER of the *C. elegans* embryo is also continuous, we generated a strain expressing the ER luminal reporter GFP::KDEL. By applying fluorescence loss in photobleaching (FLIP), we tested whether this reporter can freely diffuse throughout the entire ER or whether the ER of the one-cell embryo is subdivided into separate reservoirs. An area of interest was photobleached repeatedly between image acquisitions, and the fluorescence signal was monitored throughout the remainder of the embryo (Fig. 1 A). Photobleaching was always applied from the stage of maternal pronuclear migration until the end of the first division in either the anterior domain (32 ± 2.4% of egg length, with anterior equal to 0%) or the posterior domain (76 ± 0.5% of egg length; see Materials and methods for egg length measurements; Fig. 1 A). Over time, the fluorescence signal was lost fairly homogenously throughout the entire embryo, indicating that all regions of the cell exchanged the reporter rapidly and equally well with each other and with the photobleached area (Fig. 1 B and Videos 1 and 2). No abrupt inhomogeneity in the signal intensity was observed until cytokinesis, after which fluorescence loss was further observed in the photobleached blastomere, but not in the nonphotobleached blastomere. Thus, as observed in other systems like budding yeast, *Xenopus laevis* oocyte, and the mouse neural stem cells, the lumen of the ER is continuous throughout the one-cell embryo of *C. elegans*.

To determine whether diffusion was isotropic or more rapid in some directions than in others, we next asked whether fluorescence loss was comparable between two measurement regions equidistant to the photobleaching area, but located in such a way as to measure exchange along and perpendicular to the polarity axis of the embryo (Fig. 1 A). Measurement in the anteroposterior (A-P) axis was at 38 ± 0.9% of egg length or 70 ± 3.3% of egg length, depending on the site of the photobleached area (Fig. 1 A). To ensure the measurement regions in the A-P axis fell on the opposite domain, we used the cleavage plane at the end of the video, when the embryo has completed its first division, as the reference plane. Measurements perpendicular to the A-P axis were taken at 84% (±2.5% in anterior- and ±0.4% in posterior-bleached embryos) along an axis that crossed the middle of the photobleached area with 0% at the top of the embryo (Fig. 1 A).

After repeated photobleaching, the *GFP::KDEL* embryo lost its fluorescence at the same speed in both the A-P (Fig. 1 B, blue curves) and the perpendicular (Fig. 1 B, red curves) directions. The signal in these two measurement regions started to diverge after cytokinesis (Fig. 1 B, asterisks), when one region was in one blastomere and the other region was in the other. However, no such divergence was observed before cell division. We referred to this divergence as the anisotropy onset. Next, the kinetics of fluorescence loss of all data from the *GFP::KDEL* measurements was plotted by aligning them to the point of anisotropy onset, and we observed a similar trend in both the perpendicular and A-P directions (Fig. 1 C). This suggests that the ER luminal proteins exchange isotropically in both A-P and perpendicular directions throughout the first cell cycle, indicating that the ER network is not grossly anisotropic. Furthermore, these data confirm that the luminal fluorescent reporter diffuses freely between anterior and posterior domains of the embryo until it is physically separated by cytokinesis. Together, these data support the notion that the ER network is continuous and isotropically organized in the *C. elegans* embryo.

Exchange of ER membrane proteins between anterior and posterior domains becomes anisotropic as the cells progress toward nuclear envelope breakdown (NEBD)

We next investigated whether these conclusions also applied to the ER membrane. To study the diffusion behavior of ER membrane proteins in the *C. elegans* embryo, we used the 12-kD subunit of the signal peptidase SP12 (C34B2.10) fused to GFP (Fig. 2 A) and the ribosome-associated membrane protein 4 (RAMP4; F59F4.2) fused with YFP (Fig. 2 C; Rolls et al., 2002; Poteryaev et al., 2005; Golden et al., 2009) as reporters in FLIP assays. Unlike what we observed for the luminal marker, photobleaching of both membrane reporters caused a loss of fluorescence that was more pronounced on the half of the embryo in which the photobleached area was located than on the opposite side of the embryo. Furthermore, irrespective of the marker and whether photobleaching was applied in the anterior or posterior of the embryo, fluorescence decay was slower along the A-P direction of the embryo than along the perpendicular axis (Fig. 2, A and C; and Videos 3, 4, 5, and 6).

Precisely, fluorescence loss in the perpendicular and A-P directions showed two distinct regimes. First, fluorescence loss followed similar kinetics in both directions until a time point (Fig. 2, A and C, asterisks) generally preceding NEBD (Fig. 2, A and C, black arrowheads), indicating that in this initial phase the diffusion of the reporter was isotropic. Past that time point, the signal decay slowed in the A-P direction, whereas it was still decreasing at the same kinetics in the perpendicular direction. Thus, diffusion of the reporter had become anisotropic long before cytokinesis (Fig. 2, A and C, white arrowheads). These observations suggest that the exchange of ER membrane proteins in the A-P and the perpendicular directions is isotropic during pronuclear migration until sometime before or around NEBD. In contrast to the luminal protein, diffusion of membrane markers becomes anisotropic past NEBD and through the remainder of the division cycle (Fig. 2, A–D). This early onset of anisotropy limits the exchange along the A-P axis compared with the perpendicular axis and leads to the formation of two daughter cells with distinct levels of fluorescence intensities upon completion of division. The fact that fluorescence loss is initially uniform until sometime before NEBD demonstrates that this behavior does not simply reflect the slow speed of protein diffusion in the ER membrane.

To characterize more closely the timing with which the diffusion started to become anisotropic, we plotted the time of pronuclear meeting (PNM), NEBD, and anaphase onset for all embryos by synchronizing them to the time of furrow ingression initiation (Fig. 3 A). For both *GFP::SP12* and *RAMP4::YFP* embryos, anisotropy onset mostly preceded NEBD (Fig. 3 A), with no significant difference for this timing between the two markers. Thus, the onset of anisotropy appeared to be cell cycle dependent. To test this possibility, we depleted the B subunit of the DNA polymerase α-primase complex, DIV-1, a perturbation known to delay the cell cycle progression of the *C. elegans* embryo (Encalada et al., 2000). Indeed, the *div-1(RNAi)* embryos showed a longer cell cycle length in their first division compared with the *Ctrl(RNAi)* embryos (Fig. 3 A, green error bars), yet the time window for the anisotropy onset still took place between PNM and NEBD (Fig. 3 A). In Fig. 3 B, we compared the ratio of the time from anisotropy onset to NEBD over the time from PNM to NEBD. A ratio value >0 represented anisotropy onset occurring before NEBD, whereas a value <0 represented those after NEBD. We observed that the anisotropy onset occurred very close to NEBD for *GFP::SP12* and *RAMP4::YFP*, whereas the onset in *div-1(RNAi)* embryos was more variable and took place closer to the PNM stage (with a higher ratio value). However, the same could also be seen in the *Ctrl(RNAi)* embryos (Fig. 3 B). Therefore, we conclude that the onset of anisotropy in the ER membrane is cell cycle dependent and takes place on average shortly before NEBD.

Anisotropic exchange of ER membrane proteins is not caused by the geometric organization of the ER

We next investigated the principle underlying this anisotropy of protein diffusion in the ER membrane. We rationalized that three phenomena could explain this anisotropy: (1) discontinuity of the ER along the A-P axis, (2) a macroscopic reorganization of the ER morphology, and (3) restriction of lateral diffusion in the ER membrane somewhere between the photobleaching area and the A-P axis measurement domain by a diffusion barrier.

To ask whether this anisotropy was a consequence of ER discontinuity along the A-P axis that happened before NEBD, we examined the ER network at the NEBD stage at different planes of fixed *GFP::SP12* embryos stained for GFP. We found that the ER network was starting to concentrate around the

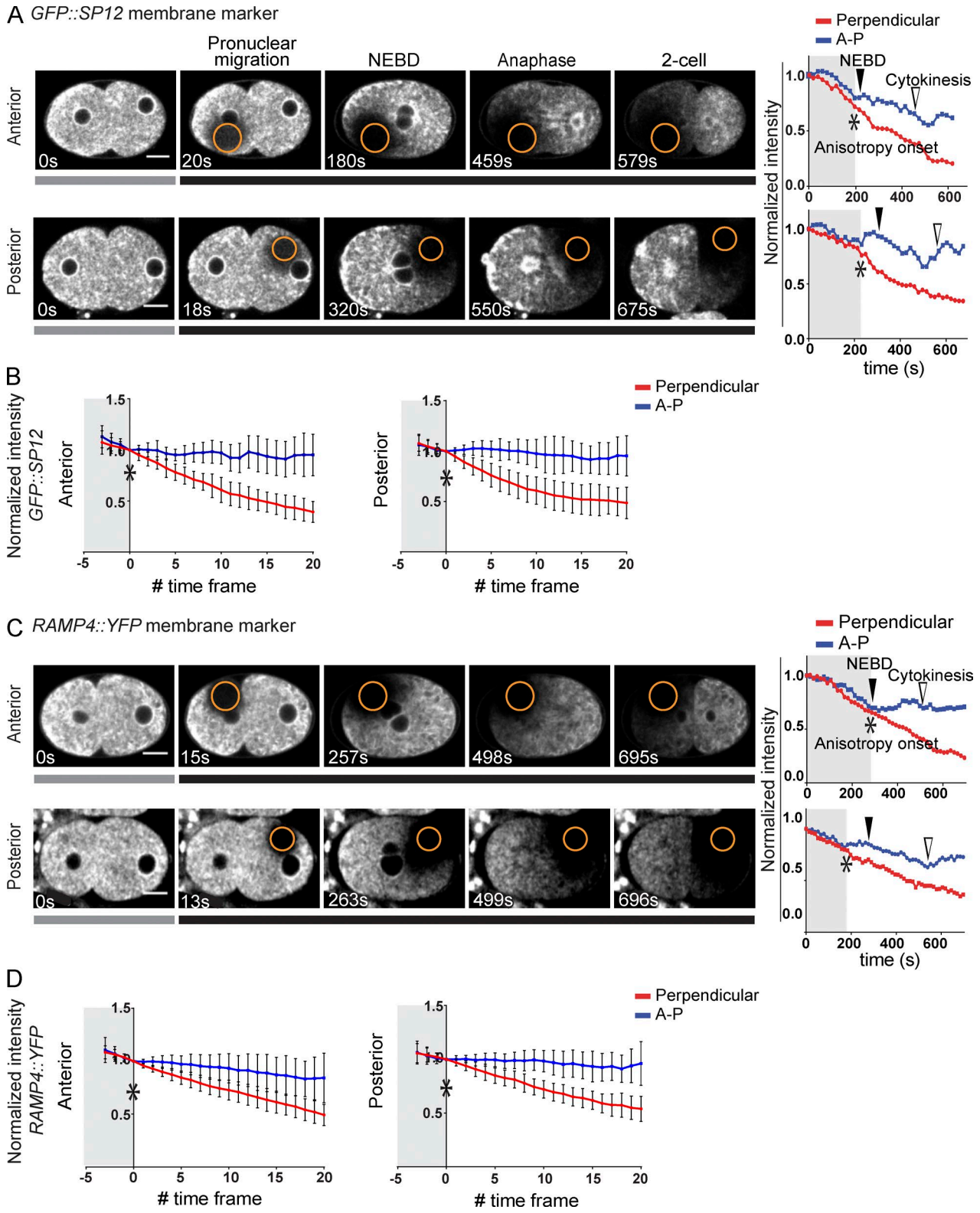

Figure 2. **The diffusion of ER membrane proteins is anisotropic in the A-P axis.** (A) Confocal images of the FLIP experiments showing a representative embryo (left) of *GFP::SP12* photobleached in the anterior or the posterior domain (orange circles). The fluorescence loss in both directions is parallel until anisotropy onset (asterisks) at a time point preceding NEBD. Also see Videos 3 and 4. (B) Graphs of the kinetics of fluorescence loss for the combined data of *GFP::SP12* embryos with the alignment to the time point of anisotropy onset. Three time points before the anisotropy onset are shown. Asterisks show the anisotropy onset. $n_{anterior}$ = 15; $n_{posterior}$ = 26. (C) Confocal images of the FLIP experiments showing a representative embryo of *RAMP4::YFP* photobleached in the anterior or the posterior domain. Also see Videos 5 and 6. (A and C) Graphs show the kinetics of fluorescence loss over time for the corresponding embryos. Gray bars indicate the prebleached first images; black bars indicate repeated bleaching in the remainder of the indicated cell cycle. The black arrowheads indicate NEBD; the white arrowheads indicate cytokinesis; gray shaded areas show the period of isotropic diffusion; asterisks show the anisotropy onset. Bars, 10 µm. (D) Graphs of the kinetics of fluorescence loss for the combined data of *RAMP4::YFP* embryos with the alignment to the time point of anisotropy onset. Graphs are as described in B. $n_{anterior}$ = 25; $n_{posterior}$ = 20. Mean ± SD.

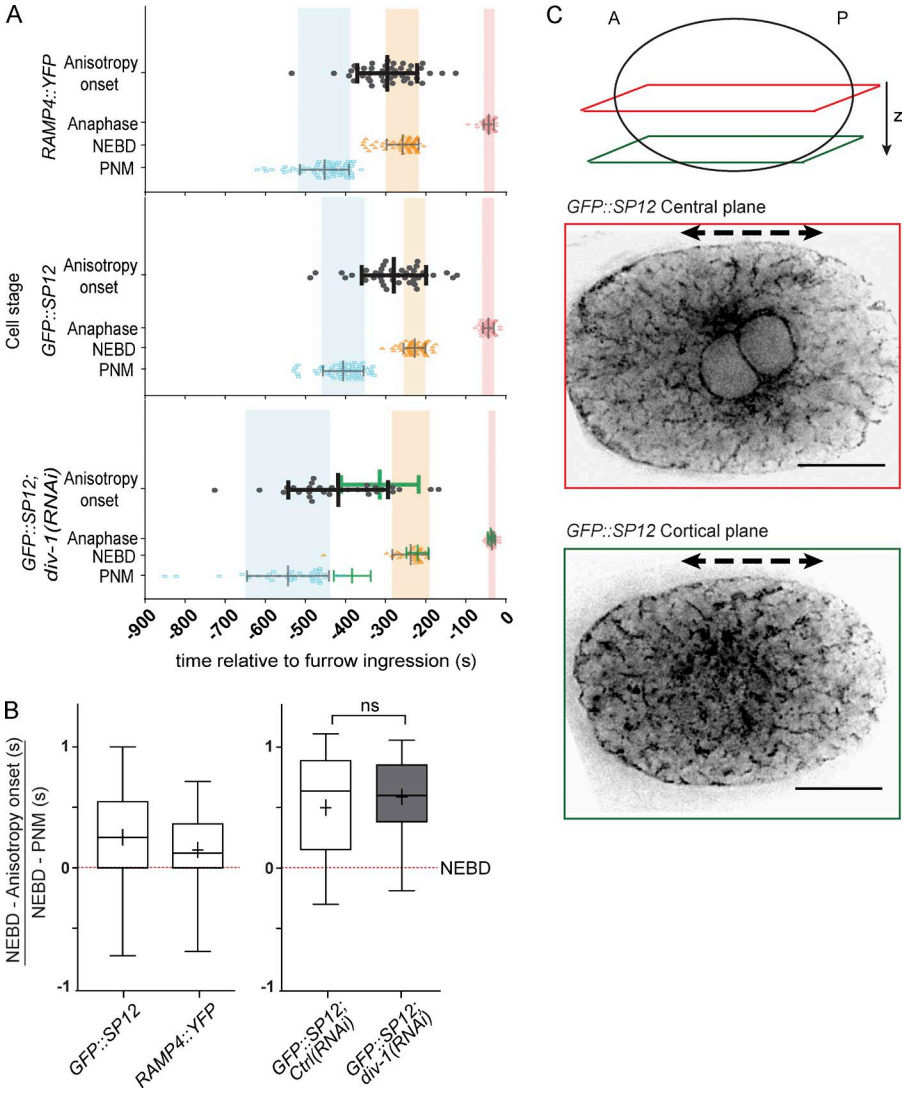

Figure 3. **The diffusion of ER membrane protein becomes anisotropic between PNM and NEBD.** (A) The timing of anisotropic diffusion onset for *GFP::SP12* (n = 57) and *RAMP4::YFP* (n = 62) relative to the cell cycle stages PNM, NEBD, and anaphase. *GFP::SP12; div-1(RNAi)* (n = 35) shows longer cell cycle length, yet the anisotropy onset occurs in the similar time window. The blue shading indicates the PNM stage, the orange shading represents NEBD, and the red shading represents anaphase. Black error bars indicate the mean ± SD of the time of anisotropy onset; gray error bars indicate the mean ± SD of the time of PNM, NEBD, and anaphase for the *RAMP::YFP* and *GFP::SP12* embryos; and green error bars indicate the mean ± SD for *GFP::SP12; Ctrl(RNAi)* (n = 34). (B) Box plots of the ratios of the time from anisotropic onset to NEBD over the time from PNM to NEBD for *GFP::SP12* (n = 42), *RAMP4::YFP* (n = 45), *GFP::SP12; div-1(RNAi)* (n = 30), and *Ctrl(RNAi)* (n = 31). Whiskers indicate the minimum and maximum values. Unpaired t test, $P < 0.05$. ns, not significant. (C) Deconvolved images of a single plane in the middle (red) and closer to the cortex (green) of the *GFP::SP12* embryo stained for GFP show the continuity of the ER membrane along the A-P axis (double-arrowed dashed line). Also see Video 7. Bars, 10 µm.

nuclei at this stage, with tubules extended out toward the cortex (Fig. 3 C and Video 7). Nonetheless, the ER was still continuous along the A-P axis both at the central and at the cortical planes, which could clearly be seen along the rim of the embryos (Fig. 3 C, double-arrowed dashed lines). Therefore, the anisotropic diffusion of the ER membrane protein is not caused by a discontinuity of the ER in the A-P axis. This finding is fully consistent with the observation that the diffusion of the luminal marker is isotropic throughout the embryo, excluding the possibility of ER discontinuity.

Dendritic ER compartmentalization was previously reported using electron microscopy (Cui-Wang et al., 2012). Although the same method has been described to study different structures in the *C. elegans* embryo (Cohen et al., 2002; O'Toole and Müller-Reichert, 2009; Hall et al., 2012; Weber et al., 2012; Woog et al., 2012; Bahmanyar et al., 2014; Serwas and Dammermann, 2015), it remains a challenge to observe the extensive ER structure while preserving its morphology. Therefore, we could not rule out that any undetected ER scission may account for a small degree of the anisotropy.

In a previous study, Poteryaev et al. (2005) reported that the macroscopic organization of the ER in the *C. elegans* embryo changes throughout the cell cycle. The ER cycles from a dispersed network in interphase, where short tubules interconnect ER patches, to a more reticulated state during mitosis. Mitotic ER consists of longer and thicker tubules with larger ER foci at the periphery, as well as sheet structures surrounding the mitotic spindle (Poteryaev et al., 2005; Gorjánácz and Mattaj, 2009). To examine whether ER anisotropy during mitosis was a consequence of these changes in ER morphology, we tested whether mutants affecting these transitions abolished the establishment of anisotropy. We applied FLIP on *lpin-1(RNAi)* and *rab-5(RNAi)* embryos, which displayed disorganized ER structures and failed to undergo normal ER morphological transitions. *lpin-1* encodes a putative phosphatidic acid phosphatase, which is homologous to human lipin. Under brightfield imaging, the down-regulation of LPIN-1 caused a reduction of lipid droplets in the embryos (Fig. 4 A). In line with previous findings (Golden et al., 2009), the ER of the *lpin-1(RNAi)* embryos appeared to be heavily patchy in severe cases, whereas in milder cases it gave a fine thready appearance (Fig. 4 A). This structure persisted from before PNM until the end of the first division (Fig. 4 C). *rab-5* is a small Rab GTPase that functions in the early endocytic pathway (McLauchlan et al., 1998; Somsel Rodman and Wandinger-Ness, 2000) and in the control of ER morphology (Audhya et al., 2007). Endogenous RAB-5 appeared in punctate structures that are concentrated in the anterior domain of the embryos and around the centrosomes, which

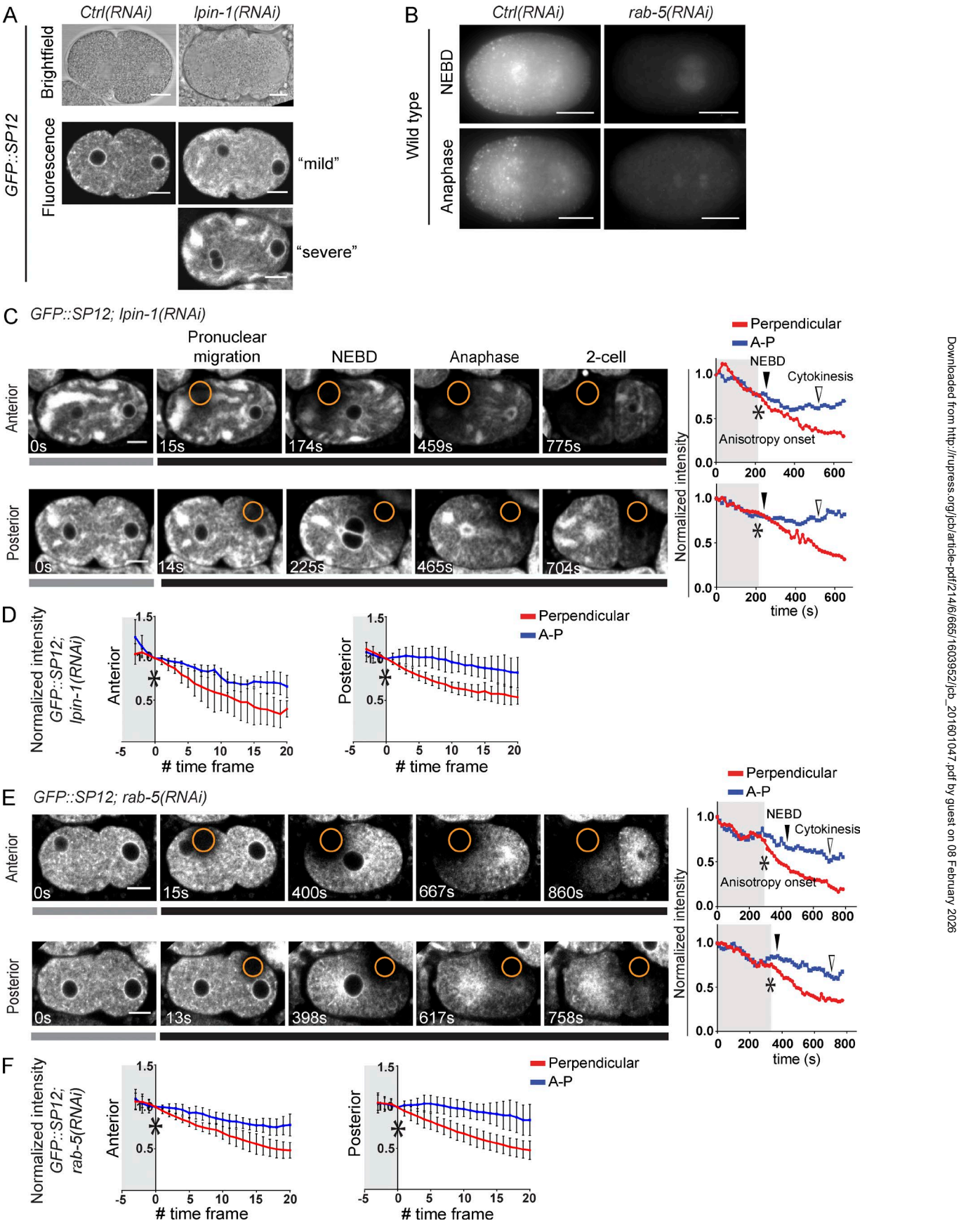

were absent upon *rab-5(RNAi)* (Fig. 4 B). The *rab-5(RNAi)* embryos exhibited a defective ER structure most prominently in mitosis in which the thick tubules and the cortical ER foci were absent (Audhya et al., 2007). In our experiment, we indeed saw the "collapsing ER" phenotype at NEBD in the *rab-5(RNAi)* embryos, which lacked cortical ER patches; furthermore, the collapsed ER also failed to return to its interphase morphology at the end of division (Fig. 4 E).

Despite these defective morphologies and the absence of the cyclic transitions, these embryos still exchanged ER membrane markers isotropically during pronuclear migration and anisotropically along the A-P axis starting shortly before NEBD, like wild-type embryos (Fig. 4, C and E; and Videos 8 and 9). After the point of anisotropy onset, the diffusion of ER membrane markers remained anisotropic until the end of the cell cycle (Fig. 4, D and F). In the ER luminal marker strain *GFP::KDEL,* the morphology of the ER was affected in a similar manner upon *lpin-1(RNAi)* and *rab-5(RNAi)* (Fig. S1, A and B). However, the kinetics of fluorescence loss in these two conditions mimicked those of the wild-type *GFP::KDEL* embryos: fluorescence was homogeneously lost throughout the embryos (Fig. S1, A–C). Thus, the observed anisotropy is not a mere consequence of the macroscopic changes of ER geometry during the cell cycle but is caused by some process taking place specifically somewhere in the membrane.

Compartmentalization of the ER membrane could explain the anisotropic diffusion of the membrane protein

We next derived a method to quantify this anisotropy. We defined an anisotropy index (AI) very similar to the barrier index used previously (Shcheprova et al., 2008; Boettcher et al., 2012; Clay et al., 2014). In short, the AI is defined by dividing the time it takes to lose 30% of the fluorescence in the A-P axis measurement domain by the time it takes to lose 30% of the fluorescence in the perpendicular measurement domain, taking the onset of anisotropy (defined as in Fig. 1) as $t = 0$ and normalizing the fluorescence to its value at that time point (Fig. 5 A). Data points after cytokinesis were not considered in the analysis. When fluorescence loss follows comparable kinetics in these two regions (indicating isotropic diffusion), the AI equals 1, whereas index values deviating from 1 reflect the extent of anisotropy.

Intriguingly, we observed that the AI value quantified for the *GFP::SP12* embryos photobleached in the posterior domain was higher than when photobleaching was applied in the anterior domain (5.0 ± 0.9 vs. 2.9 ± 0.5, $P < 0.05$; Fig. 5 B). A similar observation was made with *RAMP4::YFP*, where the AI was higher, although not significantly, when photobleaching was applied in the posterior domain (not depicted). The AI of the luminal reporter was very close to 1 irrespective of where photobleaching was applied (anterior AI = 1.2 ± 0.09 and posterior AI = 1.1 ± 0.04; Fig. 5 B). Thus, the anisotropy observed for the membrane markers was stronger when photobleaching the posterior compared with the anterior domain of the embryo. This suggested that we were observing possibly two independent processes overlying each other. On one hand, the ER membrane is organized anisotropically between the A-P and perpendicular axes, and on the other, the ER is compartmentalized into two domains of different sizes.

We first investigated whether the AI differences between posterior and anterior photobleaching could be caused by membrane fluidity being different at the anterior and at the posterior end of the embryo. To examine this possibility, we performed FRAP of *GFP::SP12* in both poles of the embryo during pronuclear migration and at NEBD. Although the diffusion of SP12 protein was not significantly faster at NEBD ($t_{1/2}$ anterior = 1.2 ± 0.1 s and posterior = 1.3 ± 0.1 s) as compared with during pronuclear migration ($t_{1/2}$ anterior = 1.4 ± 0.2 s and posterior = 1.6 ± 0.3 s), at each stage we found no significant difference between the diffusion rates measured at the anterior and posterior ends of the embryo (Fig. 5 C). Thus, the AI difference between anterior and posterior photobleaching was not caused by radical differences in ER membrane organization or in protein mobility in these two domains.

Anisotropy is only observed when the two measured areas are on opposite sides of the future cleavage plane

The one-cell embryo is polarized along the A-P axis and divides asymmetrically, giving rise to a smaller posterior and a larger anterior blastomere. If the ER was compartmentalized along this division axis, we would expect that the posterior ER domain would be smaller than the anterior one and that this would lead to a higher AI when photobleaching in the posterior than in the anterior, as we observed.

To test whether our observations could indeed be explained by compartmentalization of the ER membrane, we followed two distinct approaches. First, we asked whether the anisotropy measured was solely caused by a limited exchange of material between the anterior and posterior domains of the embryo and not by any anisotropy within each of these domains. We first photobleached an area at 32% of egg length (position 1) in the anterior domain and compared fluorescence loss either between measurement domains in the posterior (A-P axis measurement domain) and the anterior domain (perpendicular domain: Figs. 1 A and 6 A, 1x) or between measurement

Figure 4. **The anisotropic diffusion of GFP::SP12 is not caused by the macroscopic reorganization of the ER morphology.** (A) Brightfield and fluorescence images show the phenotypes of *GFP::SP12; lpin-1(RNAi)* embryos. Lipid droplets are reduced in the embryo, and the ER appears thready in milder conditions and becomes heavily patchy in severe cases. (B) *Ctrl(RNAi)* and *rab-5(RNAi)* wild-type embryos stained with α-RAB-5 antibody indicate that RAB-5 exists in punctate structures that are enriched in the anterior domain and around the centrosomes. Absence of these structures in the *rab-5(RNAi)* embryos shows that the RNAi is efficient in down-regulating the protein. Images are projection and deconvolved datasets. (C) Confocal images of the FLIP experiments showing a representative *lpin-1(RNAi)* embryo expressing GFP::SP12 photobleached in the anterior or the posterior domains (orange circles). Also see Video 8. (D) Graphs of the kinetics of fluorescence loss for the combined data of *GFP::SP12; lpin-1(RNAi)* embryos with the alignment to the time point of anisotropy onset. Three time points before the anisotropy onset are shown. Asterisks show the anisotropy onset. $n_{anterior} = 5$; $n_{posterior} = 16$. (E) Confocal images of the FLIP experiments showing a representative *rab-5(RNAi)* embryo expressing GFP::SP12 photobleached in the anterior or the posterior domains. Also see Video 9. (C and E) Graphs show the kinetics of fluorescence loss over time for the corresponding embryos. Gray bars indicate the prebleached first images; black bars indicate repeated bleaching in the remainder of the indicated cell cycle. The black arrowheads indicate NEBD; the white arrowheads indicate cytokinesis; gray shaded areas show the period of isotropic diffusion; asterisks show the anisotropy onset. (F) Graphs of the kinetics of fluorescence loss for the combined data of *GFP::SP12; rab-5(RNAi)* embryos with the alignment to the time point of anisotropy onset. Graphs are as described in D. $n_{anterior} = 17$; $n_{posterior} = 21$. Mean ± SD. Bars, 10 µm.

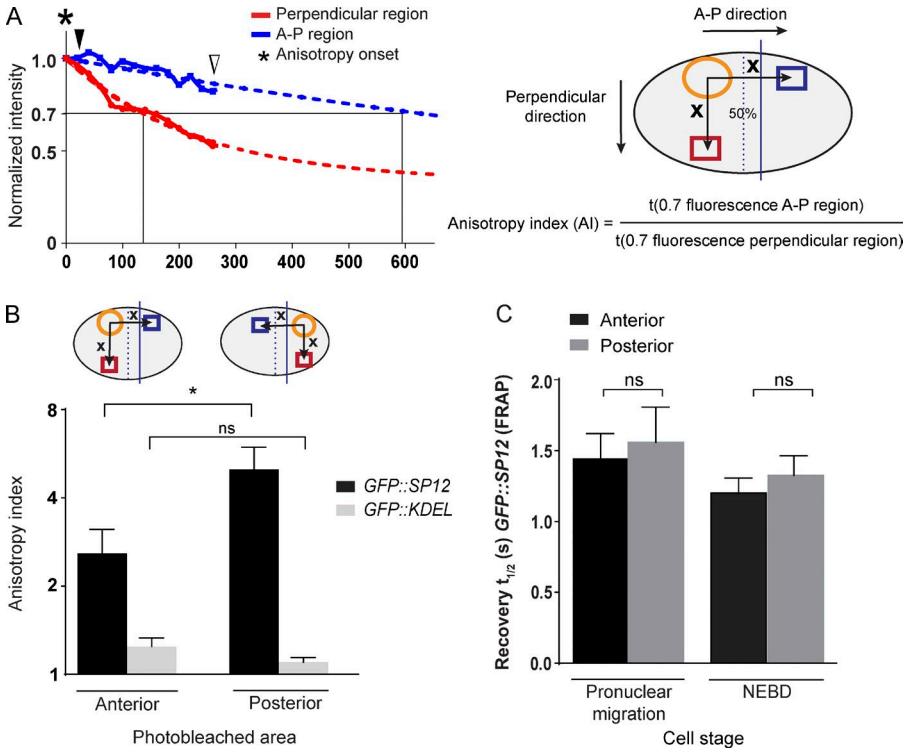

Figure 5. **The diffusion anisotropy is stronger when the posterior domain is photobleached.** (A) The quantification of anisotropy index (AI) from the kinetics of fluorescence loss. The anisotropy onset is set as time 0 and fluorescence intensity to 1.0. After fitting the kinetics of loss with one-phase decay, omitting the values after cytokinesis, the time taken for the normalized fluorescence intensity in the A-P region (blue square) to reduce to 0.7 is divided by that in the perpendicular region (red square). The black arrowhead indicates NEBD; the white arrowhead indicates cytokinesis; the orange circle indicates the photobleached area; the asterisk shows the anisotropy onset. Both measurement directions are equidistant from the photobleached area (x). (B) The AIs quantified for wild-type *GFP::SP12* ($n_{anterior}$ = 24; $n_{posterior}$ = 26) and *GFP::KDEL* ($n_{anterior}$ = 10; $n_{posterior}$ = 11). AIs shown are on $\log_2$ scale. Unpaired *t* test; *, $P < 0.05$. (C) The $t_{1/2}$ of FRAP in the anterior or the posterior domain of *GFP::SP12* embryo. $n > 20$. Mean ± SD. Unpaired *t* test, $P < 0.05$. ns, not significant.

domains both located in the anterior domain (Fig. 6 A, 1λ). In the first case, the AI reached the value of 2.9 ± 0.5 (Figs. 5 B and 6 A, 1x), whereas in the second case it decreased to 1.1 ± 0.3 (Fig. 6 A, 1λ; $P < 0.05$).

In a second set of experiments, the photobleached area was set further to the anterior at 22 ± 1.1% of egg length (position 2), mirroring the photobleached area in the posterior domain (position 3), and the same set of measurements was performed (Fig. 6 A, 2θ and 2μ). Again, when we compared fluorescence loss between two equidistant areas within the anterior domain, the obtained AI value was close to 1 (1.1 ± 0.3; Fig. 6 A, 2μ), whereas the AI value obtained using a measurement domain in the anterior and the second one in the posterior of the embryo was significantly increased (2.4 ± 0.5, $P < 0.01$; Fig. 6 A, 2θ). Note that in 2θ, the two measurement areas are not on perpendicular axes because of the necessity of keeping them equidistant from the bleaching area. The fact that keeping one measurement area on one side of the future cleavage plane and the other area on the other side is sufficient to observe a raise in anisotropy indicates that the anisotropy is indeed caused by the presence of a boundary-limiting exchange at that position and not by some orientation of the underlying ER structure. Together, these data demonstrate that diffusion was isotropic within the anterior domain and that the observed anisotropy was caused by the presence of some reduction of the exchange between the anterior and the posterior domain of the embryo.

Because of its small size, similar experiments are less demonstrative when photobleaching is applied in the posterior domain. Nonetheless, at least the fluorescence loss between two equidistant areas within the posterior domain could be measured, and the AI value was close to 1 (1.2 ± 0.1; Fig. 6 A, 3β). Interestingly, when we measured the signal just across the cleavage plane (58 ± 1.2% of egg length; Fig. 1 A) into the anterior domain and perpendicularly in the posterior domain, the AI increased significantly to 4.6 ± 0.3 (Fig. 6 A, 3γ; $P < 0.0001$). Similarly, the measurement of AI between the anterior domain across 50% of the embryo length and the posterior domain reached 5.0 ± 0.9 (Figs. 5 B and 6 A, 3x). Altogether, our data suggest that the ER of the *C. elegans* embryo is compartmentalized into a large isotropic compartment in the anterior and a small isotropic compartment in the posterior and that a lateral diffusion barrier in the ER membrane limits the exchange of material between these two compartments.

Our second approach for testing the compartmentalization model was to ask whether cortical polarity could constrain the size of the ER compartments. FLIP assays were applied to *par-3(RNAi)* embryos in the *GFP::SP12* strain. The AIs were quantified as described in Fig. 5 A. Strikingly, the values obtained upon anterior or posterior photobleaching in *par-3(RNAi)* were very similar, unlike in the controls (Fig. 6 B). However, the AI discrepancy between the anterior- and posterior-bleached embryos was still present upon *par-2(RNAi)* ($P < 0.05$; Fig. 6 B). This discrepancy indicated that the two ER compartments of the *par-2(RNAi)* embryos were still of different sizes, whereas in the *par-3(RNAi)* embryos, they became more symmetric. These data therefore suggest that polarity establishment (*par-3*), but not maintenance (*par-2*), is required to position the boundary between the two ER compartments in order to form a large anterior and a small posterior compartment. The fact that in both *par-3(RNAi)* and *par-2(RNAi)* embryos the measured AIs remain in the same range as in the controls indicates that the polarity is not required for the process of compartmentalization itself. The PAR-3 protein regulates the asymmetric distribution of various cellular components such as the early endosome, P granules, the Gβ subunit GBP-1, CDC-42 GTPase, and the G protein regulatory proteins GPR-1/2 (Tabuse et al., 1998; Colombo et al., 2003; Gotta et al., 2003; Tsou et al., 2003; Motegi and Sugimoto, 2006; Schonegg and Hyman, 2006; Andrews and Ahringer, 2007; Thyagarajan et al., 2011). Future studies will be required to identify the effectors downstream of *par-3* that control the position of the ER domain boundary.

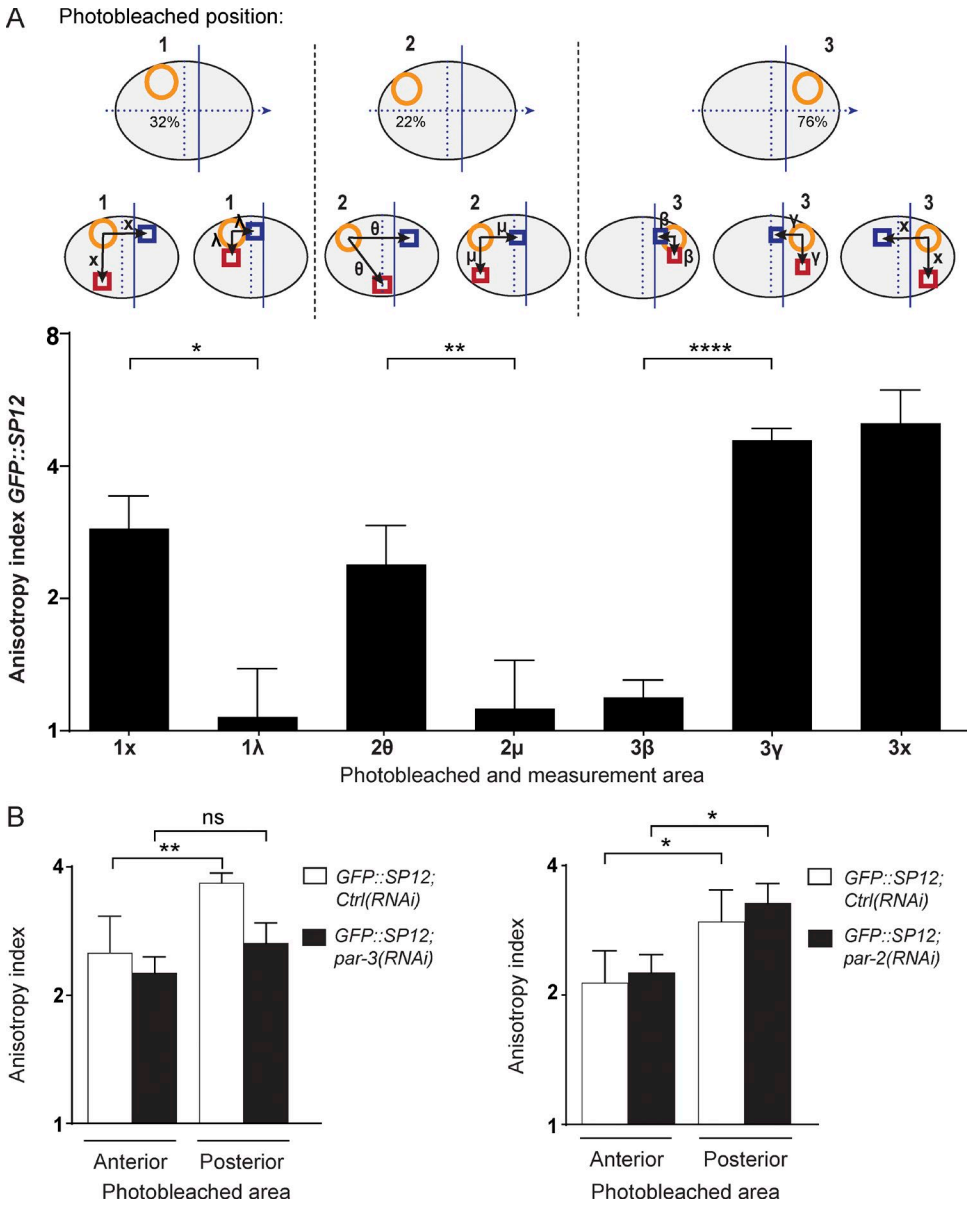

Figure 6. **The anisotropic diffusion is caused by the reduction of exchange between the ER in the anterior and posterior domains of the embryos.** The size of the ER compartments is *par-3* dependent. (A) The AIs quantified for the embryos photobleached at 32% (position 1) and 22% (position 2) of egg length in the anterior domain and 76% (position 3) of egg length in the posterior domain using the indicated measurement regions. These regions are either located in the opposite compartments (x, θ, and γ) or within the same compartment (λ, μ, and β). Orange circles indicate photobleached areas; blue squares indicate the measurement regions on the A-P axis; red squares indicate the measurement regions on the perpendicular axis. $n_{position1} \geq 19$; $n_{position2} > 34$; $n_{position3} = 26$. Mann-Whitney test; *, $P < 0.05$; **, $P < 0.01$. Unpaired *t* test; ****, $P < 0.0001$. (B) The AIs quantified for *par-3(RNAi)* ($n_{anterior} = 33$; $n_{posterior} = 28$) and *par-2(RNAi)* ($n_{anterior} = 17$; $n_{posterior} = 16$) embryos expressing GFP::SP12 in comparison with their *Ctrl(RNAi)* ($n = 17–31$). Unpaired *t* test; *, $P < 0.05$; **, $P < 0.01$. ns, not significant. All AIs shown are on $\log_2$ scale. All graphs show mean ± SD.

In summary, our study provides evidence that ER compartmentalization by a diffusion barrier is conserved in *C. elegans* embryos. The ER membrane diffusion barriers that form in budding yeast and mouse neural stem cells are shown to play a crucial role in the retention of aging factors and damages between renewing and aging cells (Clay et al., 2014; Moore et al., 2015). In our case, it will be important to elucidate the biological relevance of such barriers in an intrinsically young cell like the *C. elegans* embryo. For example, it will be interesting to investigate whether the barrier helps maintain polarity within the embryo. Therefore, uncovering the molecular nature and the mechanism of the ER diffusion barrier in the *C. elegans* embryo is now a priority in order to understand its regulation and to characterize the processes in which it is involved.

Materials and methods

Nematode strains, maintenance, and transformation

We used the following *C. elegans* strains: wild type, N2 (Bristol); WH327 *GFP::SP12*, *unc-119(ed3)* III; *ojIs23[unc-119(+); pie-1::GFP::C34B2.10]* (Poteryaev et al., 2005); JA1405 *RAMP4::YFP, unc-119(e2498)* III; and *weIs16[unc-119(+); pie-1::RAMP4::YFP]* (provided by J. Ahringer, University of Cambridge, Cambridge, England, UK). All

strains were cultured with standard procedures (Brenner, 1974). Worms were grown on nematode growth media plates and maintained at 23°C.

The *GFP::KDEL* strain was generated by fusing the signal peptide *hsp-3* (C15H9.6; first 19 amino acids) to the GFP sequence at the N terminus, followed by the KDEL retrieval sequence at the C terminus. The vector pID3.01 was modified to remove the *pie-1* promoter, and the GFP was replaced with the *mex-5* promoter (pMG742). The *GFP::KDEL* fusion sequence was cloned into the new pMG742 vector using Gateway Technology (Invitrogen). Worm transformation with the *GFP::KDEL* construct was performed using the optimized bombardment method described by Praitis et al. (2001), with the following modifications: 20 µg of plasmid DNA and 1 million *unc-119(ed3)* were used.

RNAi

RNAi bacterial clones from the library (Kamath et al., 2003) were used for the feeding method (Timmons et al., 2001). Bacteria were seeded onto NGM plates containing 100 µg/ml carbenicillin and 3 mM IPTG and were left to grow and induced overnight. For *rab-5(RNAi)*, *lpin-1(RNAi)*, and *div-1(RNAi)*, L4 hermaphrodites were fed for 48 h at 20°C. L1 hermaphrodites were used for *par-2(RNAi)* and *par-3(RNAi)* and fed for the same duration at 23°C. The L4440 empty vector was used as the control in all RNAi experiments.

FLIP and FRAP experiments

To visualize early embryos under the microscope, we extracted the embryos from the gravid worms by dissection in M9 buffer on an 18 × 18-mm coverslip. The coverslip was then inverted onto a 5% agarose pad and sealed with Vaseline. Image acquisition was done at RT (23°C) with a confocal microscope (LSM 510; ZEISS) equipped with a Plan-Neofluar 40×/1.3 NA oil immersion objective and a four–photomultiplier tubecamera. The microscope was controlled by ZEN 2008 software (ZEISS). The GFP was excited by the 488-nm line of an argon laser at 3–7% intensity and 45% output and detected with a 505-nm long-pass filter. Photobleaching was applied with 25 iterations at 100% laser power. For FLIP experiments, photobleaching was done repeatedly with the previously mentioned parameters in a region of interest (ROI) as indicated in Fig. 1 A. Positions of photobleaching were measured in percent egg length calculated as ratios of the distance from the middle of the photobleached area to the anterior pole to the total A-P length of the embryo, with the anterior equaling 0%. ROIs of diameter 13.2 µm for anterior-bleached embryos and 12.1 µm for posterior-bleached embryos were chosen. For FRAP experiments, photobleaching was applied once in an ROI of 1.32 µm in diameter for 25 frames (1 frame/s). Each experiment was repeated at least three times with a sample size of at least five.

Quantification for all the FLIP and FRAP experiments was performed with ImageJ 1.49g (National Institutes of Health). In FLIP experiments, the mean fluorescence signal was quantified in an area of the A-P and perpendicular directions as illustrated in Fig. 1 A, as well as in the neighboring embryo as a control. Positions for the quantification in the A-P direction were measured in percent egg length calculated as ratios of the distance from the middle of the blue square to the anterior pole to the total A-P length of the embryo, with the anterior equaling 0%. For positions in the perpendicular direction, ratios were calculated by the distance from the middle of the red square to the top of the embryo along the axis crossing the middle of the photobleached area to the total length of this axis. After background subtraction, the fluorescence signals in the A-P and perpendicular regions were normalized to the control embryo and set to the value of 1.0 at the start of the experiment. The data from each embryo were transferred to Prism 6.05 (GraphPad Software), where they were subjected to one-phase decay fitting by constraining the first photobleaching point to 1.0. The time needed for the A-P (unbleached) region to reduce to 0.7 was divided by that for the perpendicular (bleached) region to obtain the AI. Mean and SD values were calculated from replicated experiments. All images were processed with ImageJ 1.49g.

As for FRAP experiments, the mean fluorescence recovery signal was quantified in the photobleached ROI and a region in the neighboring control embryo. After background subtraction, the fluorescence signals of the ROI were normalized to the control embryo and set to the value of 1.0 at the start of the experiment. The data from each embryo were transferred to Prism 6.05 and fitted with a one-phase association curve from the first point of photobleach onward. Each experiment was repeated three times with $n \geq 5$. $t_{1/2}$ of fluorescence recovery to reach a plateau level for all embryos were collected, and mean and SD values were calculated from the replicated experiments.

For the measurement of the timing of anisotropic diffusion onset, data from all experiments were pooled to calculate the mean and SD. The statistical method of Student's unpaired *t* test was used to compare data that passed the Gaussian test; the Mann-Whitney test was used for data from nonnormal distribution.

Immunostaining

In the immunostaining procedures, 15–20 gravid worms were dissected in M9 buffer to release the embryos, followed by the dry ice freeze-crack methanol fixation. After fixation in −20°C methanol for 20 min, slides were rehydrated twice in PBS for 5 min. Next, we blocked the embryos with AbDil (PBS, 4% bovine serum albumin, and 0.1% Triton X-100) for 20 min at RT. Primary antibodies were then added and incubated in the dark at 4°C overnight. Slides were washed with PBT (PBS + 0.1% Triton X-100) three times, for 10 min each, before adding secondary antibodies together with DAPI and incubating in the dark for 2 h at RT. After that, slides were again washed with PBT four times, for 5 min each. Mowiol was added at the end, and slides were covered with 15 × 15-mm coverslips. The rabbit αRAB-5 antibody (1 mg/ml; provided by K. Oegema, Ludwig Institute for Cancer Research, San Diego, CA) was used in the dilution 1:1,000 together with the mouse anti–α-tubulin DM1A (Sigma-Aldrich) as a control in the staining. Mouse α-GFP antibody (Sigma-Aldrich) was used at a 1:500 dilution. Vectashield antifade mounting medium (Vector Laboratories) was used for mounting in α-GFP slides.

For the analysis of RAB-5–stained fixed embryos, we acquired images using a 60× 1.4 NA differential interference contrast oil Plan-Apo objective lens on a DeltaVision system (Applied Precision Ltd.) equipped with an IX71 base (Olympus) and a CoolSnap HQ camera (Roper Technologies) operating with the software softwoRx version 4.1.0 (Applied Precision Ltd.). Embryos at the one-cell stage were scored. Z stacks of 12 µm flanking the middle section of the embryos were imaged with an optical section spacing of 0.3 µm. The images were deconvolved (enhanced ratio) and processed for projection of max intensity. For GFP-stained embryos, images were taken on a DeltaVision OMX system (Applied Precision Ltd.) using a 60× 1.4 NA oil point spread function objective and equipped with an sCMOS MOX V4 camera (PCO) and DV OMX (3.30.43780) softwoRx version 6.0 software (Applied Precision Ltd.). Z stacks of the entire thickness of the embryo with an optical section spacing of 0.125 µm were imaged and deconvolved.

Online supplemental material

Fig. S1 displays confocal images of FLIP experiments showing representative *GFP::KDEL; lpin-1(RNAi)* and *GFP::KDEL; rab-5(RNAi)* embryos photobleached in the anterior or the posterior domain; graphs display the kinetics of fluorescence loss for the combined data of *GFP::KDEL; lpin-1(RNAi)* and *GFP::KDEL; rab-5(RNAi)* embryos

with the alignment to the time point of anisotropy onset. Videos 1 and 2 show the fluorescence signal in the corresponding *GFP::KDEL* embryo photobleached in the anterior and posterior domain, respectively (Fig. 1 B). Videos 3 and 4 show the fluorescence signal in the corresponding *GFP::SP12* embryo photobleached in the anterior and posterior domain, respectively (Fig. 2 A). Videos 5 and 6 show the fluorescence signal in the corresponding *RAMP4::YFP* embryo photobleached in the anterior and posterior domain, respectively (Fig. 2 C). Video 7 shows the ER network in the z stack deconvoluted images of the whole width of a *GFP::SP12* embryo (Fig. 3 C). Video 8 shows the fluorescence signal in the heavily patchy *GFP::SP12; lpin-1(RNAi)* embryo photobleached in the anterior domain (Fig. 4 C). Video 9 shows the fluorescence signal in the *GFP::SP12; rab-5(RNAi)* embryo photobleached in the anterior domain (Fig. 4 E) and shows the lack of cortical ER foci during mitosis. Online supplemental material is available at http://www.jcb.org/cgi/content/full/jcb.201601047/DC1.

Acknowledgments

We would like to thank Julie Ahringer and Karen Oegema for providing worm strains and reagents. We thank Fabrice Caudron for his help in using the DeltaVision OMX. We also thank the members of the Barral, Gotta, Michael Hengartner, and Alex Hajnal laboratories for discussions and suggestions and the Scientific Center for Optical and Electron Microscopy (ScopeM) of ETH Zürich for microscopy support.

Research in the laboratory of M. Gotta is funded by the University of Geneva and by the Swiss National Science Foundation (grant 31003A_156013). Work in the laboratory of Y. Barral is supported by ETH Zürich. Z.Y. Lee and Y. Barral were also supported by the grant BarrAge from the European Research Council.

The authors declare no competing financial interests.

Submitted: 15 January 2016
Accepted: 1 August 2016

References

Andrews, R., and J. Ahringer. 2007. Asymmetry of early endosome distribution in *C. elegans* embryos. *PLoS One.* 2:e493. http://dx.doi.org/10.1371/journal.pone.0000493

Audhya, A., A. Desai, and K. Oegema. 2007. A role for Rab5 in structuring the endoplasmic reticulum. *J. Cell Biol.* 178:43–56. (published erratum appears in *J. Cell Biol.* 2007. 178:1309) http://dx.doi.org/10.1083/jcb.200701139

Bahmanyar, S., R. Biggs, A.L. Schuh, A. Desai, T. Müller-Reichert, A. Audhya, J.E. Dixon, and K. Oegema. 2014. Spatial control of phospholipid flux restricts endoplasmic reticulum sheet formation to allow nuclear envelope breakdown. *Genes Dev.* 28:121–126. http://dx.doi.org/10.1101/gad.230599.113

Baumann, O., and B. Walz. 2001. Endoplasmic reticulum of animal cells and its organization into structural and functional domains. *Int. Rev. Cytol.* 205:149–214. http://dx.doi.org/10.1016/S0074-7696(01)05004-5

Blobel, G., and B. Dobberstein. 1975a. Transfer of proteins across membranes. I. Presence of proteolytically processed and unprocessed nascent immunoglobulin light chains on membrane-bound ribosomes of murine myeloma. *J. Cell Biol.* 67:835–851. http://dx.doi.org/10.1083/jcb.67.3.835

Blobel, G., and B. Dobberstein. 1975b. Transfer of proteins across membranes. II. Reconstitution of functional rough microsomes from heterologous components. *J. Cell Biol.* 67:852–862. http://dx.doi.org/10.1083/jcb.67.3.852

Boettcher, B., T.T. Marquez-Lago, M. Bayer, E.L. Weiss, and Y. Barral. 2012. Nuclear envelope morphology constrains diffusion and promotes asymmetric protein segregation in closed mitosis. *J. Cell Biol.* 197:921–937. (published erratum appears in *J. Cell Biol.* 2012. 198:143) http://dx.doi.org/10.1083/jcb.201112117

Boyd, L., S. Guo, D. Levitan, D.T. Stinchcomb, and K.J. Kemphues. 1996. PAR-2 is asymmetrically distributed and promotes association of P granules and PAR-1 with the cortex in C. elegans embryos. *Development.* 122:3075–3084.

Brenner, S. 1974. The genetics of *Caenorhabditis elegans*. *Genetics.* 77:71–94.

Clay, L., F. Caudron, A. Denoth-Lippuner, B. Boettcher, S. Buvelot Frei, E.L. Snapp, and Y. Barral. 2014. A sphingolipid-dependent diffusion barrier confines ER stress to the yeast mother cell. *eLife.* 3:e01883. http://dx.doi.org/10.7554/eLife.01883

Cohen, M., Y.B. Tzur, E. Neufeld, N. Feinstein, M.R. Delannoy, K.L. Wilson, and Y. Gruenbaum. 2002. Transmission electron microscope studies of the nuclear envelope in *Caenorhabditis elegans* embryos. *J. Struct. Biol.* 140:232–240. http://dx.doi.org/10.1016/S1047-8477(02)00516-6

Colombo, K., S.W. Grill, R.J. Kimple, F.S. Willard, D.P. Siderovski, and P. Gönczy. 2003. Translation of polarity cues into asymmetric spindle positioning in *Caenorhabditis elegans* embryos. *Science.* 300:1957–1961. http://dx.doi.org/10.1126/science.1084146

Cui-Wang, T., C. Hanus, T. Cui, T. Helton, J. Bourne, D. Watson, K.M. Harris, and M.D. Ehlers. 2012. Local zones of endoplasmic reticulum complexity confine cargo in neuronal dendrites. *Cell.* 148:309–321. http://dx.doi.org/10.1016/j.cell.2011.11.056

Dennis, E.A., and E.P. Kennedy. 1972. Intracellular sites of lipid synthesis and the biogenesis of mitochondria. *J. Lipid Res.* 13:263–267.

Encalada, S.E., P.R. Martin, J.B. Phillips, R. Lyczak, D.R. Hamill, K.A. Swan, and B. Bowerman. 2000. DNA replication defects delay cell division and disrupt cell polarity in early *Caenorhabditis elegans* embryos. *Dev. Biol.* 228:225–238. http://dx.doi.org/10.1006/dbio.2000.9965

English, A.R., and G.K. Voeltz. 2013. Endoplasmic reticulum structure and interconnections with other organelles. *Cold Spring Harbor. Perspect. Biol.* 5:a013227. http://dx.doi.org/10.1101/cshperspect.a013227

Etemad-Moghadam, B., S. Guo, and K.J. Kemphues. 1995. Asymmetrically distributed PAR-3 protein contributes to cell polarity and spindle alignment in early C. elegans embryos. *Cell.* 83:743–752. http://dx.doi.org/10.1016/0092-8674(95)90187-6

Feng, J.J., J.H. Carson, F. Morgan, B. Walz, and A. Fein. 1994. Three-dimensional organization of endoplasmic reticulum in the ventral photoreceptors of *Limulus*. *J. Comp. Neurol.* 341:172–183. http://dx.doi.org/10.1002/cne.903410204

Golden, A., J. Liu, and O. Cohen-Fix. 2009. Inactivation of the *C. elegans* lipin homolog leads to ER disorganization and to defects in the breakdown and reassembly of the nuclear envelope. *J. Cell Sci.* 122:1970–1978. http://dx.doi.org/10.1242/jcs.044743

Gorjánácz, M., and I.W. Mattaj. 2009. Lipin is required for efficient breakdown of the nuclear envelope in *Caenorhabditis elegans*. *J. Cell Sci.* 122:1963–1969. http://dx.doi.org/10.1242/jcs.044750

Gotta, M., Y. Dong, Y.K. Peterson, S.M. Lanier, and J. Ahringer. 2003. Asymmetrically distributed *C. elegans* homologs of AGS3/PINS control spindle position in the early embryo. *Curr. Biol.* 13:1029–1037. http://dx.doi.org/10.1016/S0960-9822(03)00371-3

Guo, S., and K.J. Kemphues. 1995. *par-1*, a gene required for establishing polarity in C. elegans embryos, encodes a putative Ser/Thr kinase that is asymmetrically distributed. *Cell.* 81:611–620. http://dx.doi.org/10.1016/0092-8674(95)90082-9

Hall, D.H., E. Hartwieg, and K.C. Nguyen. 2012. Modern electron microscopy methods for *C. elegans*. *Methods Cell Biol.* 107:93–149. http://dx.doi.org/10.1016/B978-0-12-394620-1.00004-7

Jaffe, L.A., and M. Terasaki. 1994. Structural changes in the endoplasmic reticulum of starfish oocytes during meiotic maturation and fertilization. *Dev. Biol.* 164:579–587. http://dx.doi.org/10.1006/dbio.1994.1225

Kamath, R.S., A.G. Fraser, Y. Dong, G. Poulin, R. Durbin, M. Gotta, A. Kanapin, N. Le Bot, S. Moreno, M. Sohrmann, et al. 2003. Systematic functional analysis of the *Caenorhabditis elegans* genome using RNAi. *Nature.* 421:231–237. http://dx.doi.org/10.1038/nature01278

Levine, T., and C. Rabouille. 2005. Endoplasmic reticulum: one continuous network compartmentalized by extrinsic cues. *Curr. Opin. Cell Biol.* 17:362–368. http://dx.doi.org/10.1016/j.ceb.2005.06.005

Luedeke, C., S.B. Frei, I. Sbalzarini, H. Schwarz, A. Spang, and Y. Barral. 2005. Septin-dependent compartmentalization of the endoplasmic reticulum during yeast polarized growth. *J. Cell Biol.* 169:897–908. http://dx.doi.org/10.1083/jcb.200412143

McLauchlan, H., J. Newell, N. Morrice, A. Osborne, M. West, and E. Smythe. 1998. A novel role for Rab5-GDI in ligand sequestration into clathrin-coated pits. *Curr. Biol.* 8:34–45. http://dx.doi.org/10.1016/S0960-9822(98)70018-1

Moore, D.L., G.A. Pilz, M.J. Araúzo-Bravo, Y. Barral, and S. Jessberger. 2015. A mechanism for the segregation of age in mammalian neural stem cells. *Science.* 349:1334–1338. http://dx.doi.org/10.1126/science.aac9868

Motegi, F., and G. Seydoux. 2013. The PAR network: redundancy and robustness in a symmetry-breaking system. *Philos. Trans. R. Soc. Lond. B Biol. Sci.* 368:20130010. http://dx.doi.org/10.1098/rstb.2013.0010

Motegi, F., and A. Sugimoto. 2006. Sequential functioning of the ECT-2 RhoGEF, RHO-1 and CDC-42 establishes cell polarity in *Caenorhabditis elegans* embryos. *Nat. Cell Biol.* 8:978–985. http://dx.doi.org/10.1038/ncb1459

Munro, E., J. Nance, and J.R. Priess. 2004. Cortical flows powered by asymmetrical contraction transport PAR proteins to establish and maintain anterior-posterior polarity in the early *C. elegans* embryo. *Dev. Cell.* 7:413–424. http://dx.doi.org/10.1016/j.devcel.2004.08.001

O'Toole, E., and T. Müller-Reichert. 2009. Electron tomography of microtubule end-morphologies in *C. elegans* embryos. *Methods Mol. Biol.* 545:135–144. http://dx.doi.org/10.1007/978-1-60327-993-2_8

Poteryaev, D., J.M. Squirrell, J.M. Campbell, J.G. White, and A. Spang. 2005. Involvement of the actin cytoskeleton and homotypic membrane fusion in ER dynamics in *Caenorhabditis elegans*. *Mol. Biol. Cell.* 16:2139–2153. http://dx.doi.org/10.1091/mbc.E04-08-0726

Praitis, V., E. Casey, D. Collar, and J. Austin. 2001. Creation of low-copy integrated transgenic lines in *Caenorhabditis elegans*. *Genetics.* 157:1217–1226.

Puhka, M., H. Vihinen, M. Joensuu, and E. Jokitalo. 2007. Endoplasmic reticulum remains continuous and undergoes sheet-to-tubule transformation during cell division in mammalian cells. *J. Cell Biol.* 179:895–909. http://dx.doi.org/10.1083/jcb.200705112

Rolls, M.M., D.H. Hall, M. Victor, E.H. Stelzer, and T.A. Rapoport. 2002. Targeting of rough endoplasmic reticulum membrane proteins and ribosomes in invertebrate neurons. *Mol. Biol. Cell.* 13:1778–1791. http://dx.doi.org/10.1091/mbc.01-10-0514

Rose, L., and P. Gönczy. 2014. Polarity establishment, asymmetric division and segregation of fate determinants in early *C. elegans* embryos. *WormBook.* 30:1–43.

Schonegg, S., and A.A. Hyman. 2006. CDC-42 and RHO-1 coordinate actomyosin contractility and PAR protein localization during polarity establishment in *C. elegans* embryos. *Development.* 133:3507–3516. http://dx.doi.org/10.1242/dev.02527

Serwas, D., and A. Dammermann. 2015. Ultrastructural analysis of *Caenorhabditis elegans* cilia. *Methods Cell Biol.* 129:341–367. http://dx.doi.org/10.1016/bs.mcb.2015.03.014

Shcheprova, Z., S. Baldi, S.B. Frei, G. Gonnet, and Y. Barral. 2008. A mechanism for asymmetric segregation of age during yeast budding. *Nature.* 454:728–734.

Somsel Rodman, J., and A. Wandinger-Ness. 2000. Rab GTPases coordinate endocytosis. *J. Cell Sci.* 113:183–192.

Tabuse, Y., Y. Izumi, F. Piano, K.J. Kemphues, J. Miwa, and S. Ohno. 1998. Atypical protein kinase C cooperates with PAR-3 to establish embryonic polarity in Caenorhabditis elegans. *Development.* 125:3607–3614.

Terasaki, M. 2000. Dynamics of the endoplasmic reticulum and golgi apparatus during early sea urchin development. *Mol. Biol. Cell.* 11:897–914. http://dx.doi.org/10.1091/mbc.11.3.897

Terasaki, M., and L.A. Jaffe. 1991. Organization of the sea urchin egg endoplasmic reticulum and its reorganization at fertilization. *J. Cell Biol.* 114:929–940. http://dx.doi.org/10.1083/jcb.114.5.929

Thyagarajan, K., K. Afshar, and P. Gönczy. 2011. Polarity mediates asymmetric trafficking of the Gβ heterotrimeric G-protein subunit GPB-1 in *C. elegans* embryos. *Development.* 138:2773–2782. http://dx.doi.org/10.1242/dev.063354

Timmons, L., D.L. Court, and A. Fire. 2001. Ingestion of bacterially expressed dsRNAs can produce specific and potent genetic interference in *Caenorhabditis elegans*. *Gene.* 263:103–112. http://dx.doi.org/10.1016/S0378-1119(00)00579-5

Tsou, M.F., A. Hayashi, and L.S. Rose. 2003. LET-99 opposes Gα/GPR signaling to generate asymmetry for spindle positioning in response to PAR and MES-1/SRC-1 signaling. *Development.* 130:5717–5730. http://dx.doi.org/10.1242/dev.00790

Vidugiriene, J., D.K. Sharma, T.K. Smith, N.A. Baumann, and A.K. Menon. 1999. Segregation of glycosylphosphatidylinositol biosynthetic reactions in a subcompartment of the endoplasmic reticulum. *J. Biol. Chem.* 274:15203–15212. http://dx.doi.org/10.1074/jbc.274.21.15203

Voeltz, G.K., M.M. Rolls, and T.A. Rapoport. 2002. Structural organization of the endoplasmic reticulum. *EMBO Rep.* 3:944–950. http://dx.doi.org/10.1093/embo-reports/kvf202

Walter, P., and G. Blobel. 1981. Translocation of proteins across the endoplasmic reticulum. II. Signal recognition protein (SRP) mediates the selective binding to microsomal membranes of in-vitro-assembled polysomes synthesizing secretory protein. *J. Cell Biol.* 91:551–556. http://dx.doi.org/10.1083/jcb.91.2.551

Walter, P., I. Ibrahimi, and G. Blobel. 1981. Translocation of proteins across the endoplasmic reticulum. I. Signal recognition protein (SRP) binds to in-vitro-assembled polysomes synthesizing secretory protein. *J. Cell Biol.* 91:545–550. http://dx.doi.org/10.1083/jcb.91.2.545

Watts, J.L., B. Etemad-Moghadam, S. Guo, L. Boyd, B.W. Draper, C.C. Mello, J.R. Priess, and K.J. Kemphues. 1996. Par-6, a gene involved in the establishment of asymmetry in early C. elegans embryos, mediates the asymmetric localization of PAR-3. *Development.* 122:3133–3140.

Weber, B., G. Greenan, S. Prohaska, D. Baum, H.C. Hege, T. Müller-Reichert, A.A. Hyman, and J.M. Verbavatz. 2012. Automated tracing of microtubules in electron tomograms of plastic embedded samples of *Caenorhabditis elegans* embryos. *J. Struct. Biol.* 178:129–138. http://dx.doi.org/10.1016/j.jsb.2011.12.004

Woog, I., S. White, M. Büchner, M. Srayko, and T. Müller-Reichert. 2012. Correlative light and electron microscopy of intermediate stages of meiotic spindle assembly in the early *Caenorhabditis elegans* embryo. *Methods Cell Biol.* 111:223–234. http://dx.doi.org/10.1016/B978-0-12-416026-2.00012-1